# Online Supplemental Appendix to: Estimating Correlations and Reading the News by Candlesticks

Tim Bollerslev* Jia Li† Qiyuan Li‡ Yifan Li§

May 7, 2026

**Abstract**

This supplemental appendix is divided into two sections. Section SA discusses a general minimaxity result in the quadratic consistent class of correlation estimators. Section SB presents additional simulation results.

*Department of Economics, Duke University, Durham, NC 27708, and NBER; e-mail: boller@duke.edu.
†School of Economics, Singapore Management University; e-mail: jiali@smu.edu.sg.
‡Faculty of Business and Economics, University of Hong Kong; e-mail: qiyuanli@hku.hk.
§Accounting & Finance Division, University of Manchester; e-mail: yifan.li@manchester.ac.uk.

## SA (Near) Minimaxity in the Quadratic Consistent Class

Our numerical results in Figure 2 of the main text indicate that $\widetilde{V}(\lambda;\rho)$ is nonincreasing in $|\rho|$ for every $\lambda \in [0,1]$, and in particular at $\lambda^*$. A more granular numerical illustration is presented in Figure S1. Unfortunately, verifying this monotonicity condition requires new analytical results for the fourth moments of correlated Brownian motions, which are not yet available in the literature. However, under the weaker condition that $\widetilde{V}(\lambda;0) \geq \widetilde{V}(\lambda;\rho)$ for all $\rho \in [-1,1]$, we shall show that the claimed minimaxity result in the main text actually holds over a much wider class than the current one-parameter class of estimators $\mathcal{E}_{\mathrm{L}} = \{\hat{\rho}_n(\lambda) : \lambda \in [0,1]\}$.

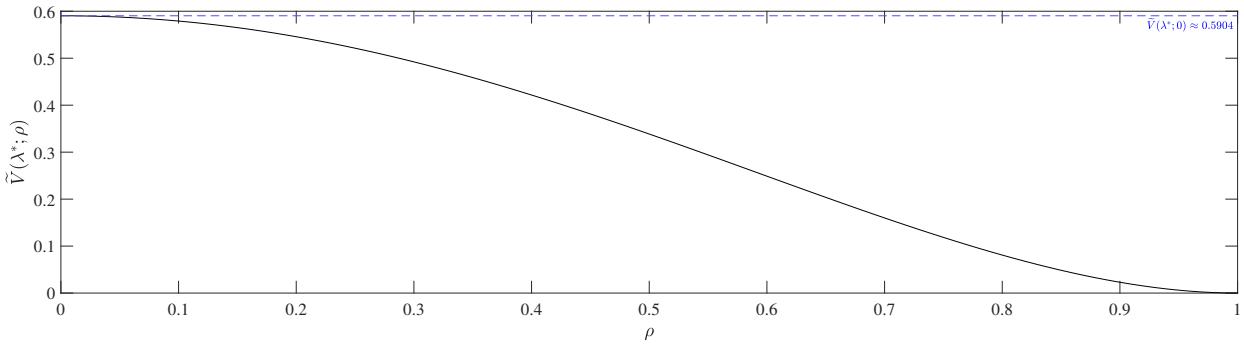


Figure S1: Numerically computed $\widetilde{V}(\lambda^*;\rho)$. The moments in $V_{\lambda^*}(\rho)$ are simulated from $10^7$ realizations of bivariate Brownian paths with $10^6$ Euler discretization steps.

To fix ideas, let us define the vector of averaged quadratic normalized candlestick features

$$X_n = \frac{1}{k_n \Delta_n} \sum_{i=1}^{k_n} \big(C_{n,i}^{(1)} C_{n,i}^{(2)}, A_{n,i}^{(1)} A_{n,i}^{(2)}, (C_{n,i}^{(1)})^2, (A_{n,i}^{(1)})^2, (C_{n,i}^{(2)})^2, (A_{n,i}^{(2)})^2\big)^\top,$$

associated with the moment vector

$$m(\Sigma) \equiv \big(\sigma^{(1)}\sigma^{(2)}\rho, \sigma^{(1)}\sigma^{(2)} g_A(\rho), (\sigma^{(1)})^2, (\sigma^{(1)})^2\theta_1, (\sigma^{(2)})^2, (\sigma^{(2)})^2\theta_1\big)^\top,$$

where $\Sigma$ is the 2-by-2 variance-covariance matrix with volatilities $\sigma^{(1)}$, $\sigma^{(2)}$ and correlation $\rho$, $g_A(\rho) = 2\big(c(\rho) - c(-\rho)\big) - \rho$, and $\theta_\lambda = 1 + 2\lambda(1 - 2\log 2)$. Note that $m(\Sigma) = \mathbb{E}[\zeta_{X,1}(\Sigma)]$ with

$$\zeta_{X,1}(\Sigma) \equiv \big(\sigma^{(1)}\sigma^{(2)}\zeta_{C,1}^{(1)}\zeta_{C,1}^{(2)}, \sigma^{(1)}\sigma^{(2)}\zeta_{A,1}^{(1)}\zeta_{A,1}^{(2)}, (\sigma^{(1)}\zeta_{C,1}^{(1)})^2, (\sigma^{(1)}\zeta_{A,1}^{(1)})^2, (\sigma^{(2)}\zeta_{C,1}^{(2)})^2, (\sigma^{(2)}\zeta_{A,1}^{(2)})^2\big)^\top,$$

where $(\zeta_{C,1}^{(1)}\zeta_{C,1}^{(2)}, \zeta_{A,1}^{(1)}\zeta_{A,1}^{(2)})$ are constructed from a bivariate Brownian motion with correlation $\rho$.

For any function $h : \mathbb{R}^6 \to [-1,1]$, define a candidate spot correlation estimator as:

$$\hat{\rho}_n(h) = h(X_n).$$

For $\hat{\rho}_n(h)$ to be a well-behaved correlation estimator, we impose some regularity conditions on $h$.

Define the open domain in $\mathbb{R}^6$:

$$U = \{x \in \mathbb{R}^6 : x_3 \wedge x_4 \wedge x_5 \wedge x_6 > 0, x_1^2 < x_3 x_5, x_2^2 < x_4 x_6\},$$

and let $\mathcal{M} := \{m(\Sigma) : \Sigma \in S_{++}^2\} \subset U$, where $S_{++}^2$ is the 2-by-2 positive-definite cone. We define the class $\mathcal{H}_{\mathrm{QC}}$ as the set of functions $h : U \to [-1, 1]$ such that:

1. $h$ is continuously differentiable on $U$;
2. $h$ satisfies the consistency condition

$$h\big(m(\Sigma)\big) = \rho, \qquad \forall \Sigma \in S_{++}^2,$$

   where $\rho$ is the associated correlation coefficient of $\Sigma$;

3. $h$ is scale-invariant:

$$h(q_1 q_2 x_1, q_1 q_2 x_2, q_1^2 x_3, q_1^2 x_4, q_2^2 x_5, q_2^2 x_6) = h(x)$$

   for all $q_1, q_2 > 0$ and all $x \in U$.

In particular, writing $\Sigma = D^{1/2} R_\rho D^{1/2}$, where $D$ is the diagonal matrix of variances and $R_\rho$ is the associated correlation matrix, then the scale-invariance and consistency conditions of $h$ implies

$$h\big(m(\Sigma)\big) = h\big(m(R_\rho)\big) = \rho.$$

We define the following quadratic consistent class of correlation estimators as

$$\mathcal{E}_{\mathrm{QC}} \equiv \{\hat{\rho}_n(h) : h \in \mathcal{H}_{\mathrm{QC}}\}.$$

The class $\mathcal{E}_{\mathrm{QC}}$ clearly nests the linear class of estimators with $\mathcal{E}_{\mathrm{L}} \subset \mathcal{E}_{\mathrm{QC}}$. It also includes any (possibly infinite) convex combinations of elements in $\mathcal{E}_{\mathrm{L}}$, such as the Popov estimator $\hat{\rho}_{P,n} = \big(\hat{\rho}_n(0) + \hat{\rho}_n(1)\big)/2$, as well as consistent modifications of linear combinations of the inconsistent spot correlation estimators in $\{\hat{\varrho}_n(\lambda) : \lambda \in [0, 1]\}$. Consequently, it covers a substantially larger class of estimators than those studied in this paper.

By Theorem 1 and the multivariate delta method, it is straightforward to show that all elements in $\mathcal{E}_{\mathrm{QC}}$ are consistent and $\mathcal{F}_\tau$-conditionally Gaussian. To present the limit law, we introduce some further notation. Denote $m_\tau \equiv m(\Sigma_\tau)$, and write $\nabla h(m_\tau)$ as the 6-by-1 gradient vector of $h$ evaluated at $m_\tau$. Define the following conditional variance-covariance matrix:

$$\mathsf{Var}[\zeta_{X,1}(R_{\rho_\tau}) \mid \mathcal{F}_\tau] = \Omega_\tau,$$

where $R_\rho$ is the 2-by-2 correlation matrix with correlation coefficient $\rho$, and write $\widetilde{V}_{\mathrm{QC}}(h;\rho_\tau) \equiv \nabla h(m_\tau)^\top \Omega_\tau \nabla h(m_\tau)$. Note that $\widetilde{V}_{\mathrm{QC}}(h;\rho_\tau)$ depends on $\Sigma_\tau$ only through $\rho_\tau$ due to the scale-invariance of $h$. We have the following result:

**Corollary S1.** *Under the same conditions as the consistency result of Theorem 1, it holds for all fixed $h \in \mathcal{H}_{QC}$ that*

$$\hat{\rho}_n(h) \xrightarrow{\mathbb{P}} \rho_\tau.$$

*Furthermore, under the same condition as the $\mathcal{F}_\tau$-conditional CLT of Theorem 1:*

$$\sqrt{k_n}\big(\hat{\rho}_n(h) - \rho_\tau\big) \xrightarrow{\mathcal{L}|\mathcal{F}_\tau} \sqrt{\widetilde{V}_{\mathrm{QC}}(h;\rho_\tau)}Z,$$

*where $Z \sim \mathcal{N}(0,1)$ is defined on an extension of $\big(\Omega, (\mathcal{F}_t)_{t\geq 0}, \mathcal{F}, \mathbb{P}\big)$ independent of $\mathcal{F}$.*

We now show that, under the numerically verified inequality $\widetilde{V}(\lambda;0) \geq \widetilde{V}(\lambda;\rho)$, our proposed estimator $\hat{\rho}_n^*$ is in fact minimax in the class $\mathcal{E}_{\mathrm{QC}}$.

**Theorem S1.** *Suppose $\widetilde{V}(\lambda^*;\rho) \leq \widetilde{V}(\lambda^*;0), \forall \rho \in (-1,1)$. Then*

$$\inf_{h\in\mathcal{H}_{\mathrm{QC}}} \sup_{\rho\in(-1,1)} \widetilde{V}_{\mathrm{QC}}(h;\rho) = \sup_{\rho\in(-1,1)} \widetilde{V}(\lambda^*;\rho) = \widetilde{V}(\lambda^*;0).$$

*Thus $\hat{\rho}_n^* = \hat{\rho}_n(\lambda^*)$ is asymptotically minimax within the quadratic consistent class $\mathcal{E}_{\mathrm{QC}}$.*

## SA.1 Proofs of Corollary S1 and Theorem S1

*Proof of Corollary S1.* Define the following coupled version of $X_n$:

$$\widetilde{X}_n \equiv \frac{1}{k_n}\sum_{i=1}^{k_n} \big(\widetilde{C}_{n,i}^{(1)}\widetilde{C}_{n,i}^{(2)}, \widetilde{A}_{n,i}^{(1)}\widetilde{A}_{n,i}^{(2)}, (\widetilde{C}_{n,i}^{(1)})^2, (\widetilde{A}_{n,i}^{(1)})^2, (\widetilde{C}_{n,i}^{(2)})^2, (\widetilde{A}_{n,i}^{(2)})^2\big)^\top.$$

By the same proof as Lemma A.6, we have the following coupling relation

$$\|X_n - \widetilde{X}_n\|_1 = O_p(\Delta_n^{1/2\wedge(1-\beta)\kappa}). \tag{SA.1}$$

Furthermore, by the same proof as Lemma A.7, for $\beta \in (0,1)$ we deduce

$$\widetilde{X}_n \xrightarrow{\mathbb{P}} m(\Sigma_\tau).$$

The coupling relation in (SA.1) and the continuous mapping lemma allow us to pass the convergence to the observed candlestick feature vector:

$$X_n \xrightarrow{\mathbb{P}} m(\Sigma_\tau).$$

Finally, for any $h \in \mathcal{H}_{\mathrm{QC}}$, by the continuity of $h$ at $m(\Sigma_\tau)$ and the consistency condition of $h$, we deduce:

$$\hat{\rho}_n(h) = h(X_n) \xrightarrow{\mathbb{P}} h\big(m(\Sigma_\tau)\big) = \rho_\tau, \tag{SA.2}$$

which proves the consistency of $\hat{\rho}_n(h) \in \mathcal{E}_{\mathrm{QC}}$.

For the conditional CLT, following similar steps as the proof of (A.17), with $\beta < 2\kappa/(2\kappa+1)$ we also deduce the following multivariate $\mathcal{F}_\tau$-conditional CLT:

$$\sqrt{k_n}\big(\widetilde{X}_n - m(\Sigma_\tau)\big) \xrightarrow{\mathcal{L}|\mathcal{F}_\tau} Z_\tau,$$

where $Z_\tau$ is a centered conditionally Gaussian vector with the $\mathcal{F}_\tau$-conditional covariance matrix $\mathsf{Var}[\zeta_{X,1}(\Sigma_\tau) \mid \mathcal{F}_\tau]$. By (SA.1) and the asymptotic equivalence lemma, we can also pass this hexvariate CLT to the observed candlestick feature vector:

$$\sqrt{k_n}\big(X_n - m(\Sigma_\tau)\big) \xrightarrow{\mathcal{L}|\mathcal{F}_\tau} Z_\tau. \tag{SA.3}$$

Now take any $h \in \mathcal{H}_{\mathrm{QC}}$. Since $h$ is continuously differentiable at $m(\Sigma_\tau)$ by assumption, applying the multivariate delta method to the above conditional CLT yields

$$\sqrt{k_n}\big(\hat{\rho}_n(h) - \rho_\tau\big) = \sqrt{k_n}\big(h(X_n) - h(m(\Sigma_\tau))\big) \xrightarrow{\mathcal{L}|\mathcal{F}_\tau} \nabla h(m_\tau)^\top Z_\tau,$$

and it suffices to notice that $\nabla h(m_\tau)^\top Z_\tau$ and $\sqrt{\widetilde{V}_{\mathrm{QC}}(h;\rho_\tau)}Z$ are equal in $\mathcal{F}_\tau$-conditional law by the scale invariance of $h$. This completes the proof. □

*Proof of Theorem S1.* We first establish a lower bound for the risk at $\rho = 0$. Let $R_\rho$ denote the 2-by-2 correlation matrix identified by $\rho \in (-1,1)$, and hence $R_0$ is the 2-dimensional identity matrix. Define

$$m_\rho \equiv m(R_\rho) = \big(\rho, g_A(\rho), 1, \theta_1, 1, \theta_1\big)^\top.$$

Fix any $h \in \mathcal{H}_{\mathrm{QC}}$, and write $d \equiv \nabla h(m_0) = (d_1, \ldots, d_6)^\top$, which exists due to the continuous differentiability of $h$ on $U$. By the consistency condition on $h$:

$$h\big(m(R_\rho)\big) = \rho, \qquad \rho \in (-1,1).$$

Differentiating this identity at $\rho = 0$ gives $d_1 + \eta d_2 = 1$, where $\eta \equiv g_A'(0) = 4c'(0) - 1 = 1 - 8/\pi^2$.

In the conditional CLT of Corollary S1 and using the scale-invariance of $h$, the influence variable of $h$ at $\rho_\tau = 0$ is

$$\psi_h(0) = d^\top\big(\zeta_{X,1}(R_0) - m_0\big),$$

such that $\widetilde{V}_{\mathrm{QC}}(h;0) = \mathsf{Var}\big(\psi_h(0)\big)$, which takes the explicit form

$$\psi_h(0) = d_1 T_C + d_2 T_A + D_h,$$

where $T_C \equiv \zeta_{C,1}^{(1)}\zeta_{C,1}^{(2)}$, $T_A \equiv \zeta_{A,1}^{(1)}\zeta_{A,1}^{(2)}$, and

$$D_h = d_3\big((\zeta_{C,1}^{(1)})^2 - 1\big) + d_4\big((\zeta_{A,1}^{(1)})^2 - \theta_1\big) + d_5\big(\zeta_{C,1}^{(2)})^2 - 1\big) + d_6\big((\zeta_{A,1}^{(2)})^2 - \theta_1\big).$$

At $\rho = 0$, the two Brownian paths are independent. Hence $\mathsf{Var}(T_C) = 1$, $\mathsf{Var}(T_A) = \theta_1^2$, and $\mathsf{Cov}(T_C, T_A) = 0$. Also, $D_h$ is uncorrelated with $T_C$ and $T_A$, because each term in $D_h$ depends on only one Brownian path and

$$\mathbb{E}[\zeta_C^{(j)}] = \mathbb{E}[\zeta_A^{(j)}] = 0, \quad j \in \{1, 2\}.$$

Therefore,

$$\widetilde{V}_{\mathrm{QC}}(h; 0) = \mathsf{Var}\big(\psi_h(0)\big) = d_1^2 + \theta_1^2 d_2^2 + \mathrm{Var}(D_h) \geq d_1^2 + \theta_1^2 d_2^2.$$

Since $d_1 + \eta d_2 = 1$, the Cauchy–Schwarz inequality yields

$$1 = (d_1 + \eta d_2)^2 \leq (d_1^2 + \theta_1^2 d_2^2)\Big(1 + \frac{\eta^2}{\theta_1^2}\Big).$$

Thus, for every $h \in \mathcal{H}_{\mathrm{QC}}$, we have

$$\widetilde{V}_{\mathrm{QC}}(h; 0) \geq d_1^2 + \theta_1^2 d_2^2 \geq \frac{\theta_1^2}{\theta_1^2 + \eta^2},$$

which further implies that

$$\inf_{h \in \mathcal{H}_{\mathrm{QC}}} \sup_{\rho \in (-1,1)} \widetilde{V}_{\mathrm{QC}}(h; \rho) \geq \inf_{h \in \mathcal{H}_{\mathrm{QC}}} \widetilde{V}_{\mathrm{QC}}(h; 0) \geq \frac{\theta_1^2}{\theta_1^2 + \eta^2}. \tag{SA.4}$$

We now show that the lower bound is attained by the proposed estimator $\hat{\rho}_n^*$. We first verify rigorously that the class of estimator $\hat{\rho}_n(\lambda) \in \mathcal{E}_{\mathrm{QC}}$ for all $\lambda \in [0, 1]$. For each $\lambda \in [0, 1]$, define the mapping

$$\Phi_\lambda(x) \equiv \frac{(1-\lambda)x_1 + \lambda x_2}{\sqrt{\{(1-\lambda)x_3 + \lambda x_4\}\{(1-\lambda)x_5 + \lambda x_6\}}}.$$

It is clear that $\Phi_\lambda(x) \in (-1, 1)$ for all $x \in U$ and is continuously differentiable on $U$. Set $h_\lambda(x) = (g_\lambda^{-1} \circ \Phi_\lambda)(x)$, so that $\hat{\rho}_n(h_\lambda) \equiv \hat{\rho}_n(\lambda)$ for $\lambda \in [0, 1]$. By Lemma A.2, the continuous differentiability of $g_\lambda^{-1}$ on $(-1, 1)$ further implies that $h_\lambda$ is continuously differentiable on $U$. The functional form of $\Phi_\lambda$ also ensures that $h_\lambda$ is scale-invariant on $U$. Moreover, for any $\Sigma \in S_{++}^2$ with the decomposition $\Sigma = D^{1/2} R_\rho D^{1/2}$, we have

$$\Phi_\lambda\big(m(\Sigma)\big) = \Phi_\lambda\big(m(R_\rho)\big) = g_\lambda(\rho).$$

Therefore, $h_\lambda(m(\Sigma)) = (g_\lambda^{-1} \circ \Phi_\lambda)(m(\Sigma)) = (g_\lambda^{-1} \circ g_\lambda)(\rho) = \rho$, so $h_\lambda$ satisfies the consistency condition. As a result, $h_\lambda \in \mathcal{H}_{\mathrm{QC}}$, and hence $\hat{\rho}_n(\lambda) \in \mathcal{E}_{\mathrm{QC}}$, for each $\lambda \in [0, 1]$.

At $\rho = 0$ and since $g_\lambda(0) = 0$, the influence variable of $h_\lambda$ simplifies to:

$$\psi_{h_\lambda}(0) = \frac{\zeta_\lambda^{(1,2)}}{g'_\lambda(0)} = \frac{(1-\lambda)T_C + \lambda T_A}{(1-\lambda) + \lambda\eta} \equiv a_\lambda T_C + b_\lambda T_A,$$

satisfying $a_\lambda + \eta b_\lambda = 1$. Thus the coefficient ratio is

$$\frac{b_\lambda}{a_\lambda} = \frac{\lambda}{1-\lambda}.$$

In the quadratic lower bound, the corresponding coefficients satisfy $d_1 + \eta d_2 = 1$ and

$$\frac{d_2}{d_1} = \frac{\eta}{\theta_1^2}.$$

Therefore, the one-parameter estimator $\hat{\rho}_n(\lambda)$ attaining the lower bound has $\lambda^*$ that satisfies

$$\frac{\lambda^*}{1-\lambda^*} = \frac{\eta}{\theta_1^2},$$

or equivalently $\lambda^* = \eta/(\eta + \theta_1^2)$. But this is simply the optimal $\lambda^*$ for the class $\mathcal{E}_{\mathrm{L}}$, which can be readily seen from its closed-form formula in (13):

$$\lambda^* = \frac{4c'(0) - 1}{4c'(0) - 1 + (3 - 4\log 2)^2} \equiv \frac{\eta}{\eta + \theta_1^2}.$$

Therefore, for the choice $h_{\lambda^*} \in \mathcal{H}_{\mathrm{QC}}$, we have

$$\widetilde{V}_{\mathrm{QC}}(h_{\lambda^*}; 0) = \frac{\theta_1^2}{\theta_1^2 + \eta^2} = \widetilde{V}(\lambda^*; 0).$$

By the assumed worst-case-at-zero condition,

$$\sup_{\rho \in (-1,1)} \widetilde{V}_{\mathrm{QC}}(h_{\lambda^*}; \rho) = \sup_{\rho \in (-1,1)} \widetilde{V}(\lambda^*; \rho) = \widetilde{V}(\lambda^*; 0).$$

Therefore,

$$\inf_{h \in \mathcal{H}_{\mathrm{QC}}} \sup_{\rho \in (-1,1)} \widetilde{V}_{\mathrm{QC}}(h; \rho) \leq \sup_{\rho \in (-1,1)} \widetilde{V}_{\mathrm{QC}}(h_{\lambda^*}; \rho) = \widetilde{V}(\lambda^*; 0).$$

Combining this upper bound with the lower bound proved in (SA.4) gives

$$\inf_{h \in \mathcal{H}_{\mathrm{QC}}} \sup_{\rho \in (-1,1)} \widetilde{V}_{\mathrm{QC}}(h; \rho) = \sup_{\rho \in (-1,1)} \widetilde{V}_{\mathrm{QC}}(h_{\lambda^*}; \rho) = \widetilde{V}(\lambda^*; 0).$$

This completes the proof. □

## SB Additional Simulation Results

This section presents additional simulation evidence supporting Section 3 of the main text. Tables S1 and S2 report the simulated bias, variance, and relative MSE of $\hat{\rho}_n^*$, $\hat{\rho}_{C,n}$, and $\hat{\rho}_{P,n}$ under the balanced sampling design with $(\lambda^{(1)}, \lambda^{(2)}) = (1000, 1000)$ and the extreme-asynchronicity design with $(\lambda^{(1)}, \lambda^{(2)}) = (1000, 100)$, respectively, complementing Table 2 of the main text. The sign accuracies for $\hat{\rho}_n^*$, $\hat{\rho}_{C,n}$, and $\hat{\rho}_{P,n}$ under the balanced sampling design with $(\lambda^{(1)}, \lambda^{(2)}) = (1000, 1000)$ and the extreme-asynchronicity design with $(\lambda^{(1)}, \lambda^{(2)}) = (1000, 100)$ are presented in Figure S2, complementing Figure 5 of the main text. The finite sample coverage rates for the 95% fixed-$k$ and large-$k$ confidence intervals of $\hat{\rho}_n^*$ under $(\lambda^{(1)}, \lambda^{(2)}) \in \{(1000, 1000), (1000, 100)\}$ are presented in Figure S3, complementing Figure 6 of the main text.

| | Bias | | | Variance ×100 | | | Relative MSE | |
|---|---|---|---|---|---|---|---|---|
| | $\hat{\rho}_n^*$ | $\hat{\rho}_{C,n}$ | $\hat{\rho}_{P,n}$ | $\hat{\rho}_n^*$ | $\hat{\rho}_{C,n}$ | $\hat{\rho}_{P,n}$ | $\hat{\rho}_n^*$ | $\hat{\rho}_{P,n}$ |
| Panel 1: $\gamma = 0, (\lambda^{(1)}, \lambda^{(2)}) = (1000, 1000)$ | | | | | | | | |
| $k = 5$ | -0.023 | -0.038 | -0.048 | 9.704 | 15.392 | 10.252 | 0.538 | 0.596 |
| $k = 10$ | -0.011 | -0.017 | -0.023 | 6.248 | 8.693 | 6.454 | 0.571 | 0.611 |
| $k = 30$ | -0.005 | -0.006 | -0.009 | 4.099 | 4.841 | 4.150 | 0.596 | 0.625 |
| $k = 60$ | -0.003 | -0.004 | -0.006 | 3.559 | 3.900 | 3.583 | 0.612 | 0.633 |
| Panel 2: $\gamma = 0.5, (\lambda^{(1)}, \lambda^{(2)}) = (1000, 1000)$ | | | | | | | | |
| $k = 5$ | -0.022 | -0.036 | -0.048 | 9.699 | 15.742 | 10.365 | 0.525 | 0.596 |
| $k = 10$ | -0.013 | -0.019 | -0.026 | 6.181 | 8.769 | 6.383 | 0.552 | 0.599 |
| $k = 30$ | -0.005 | -0.007 | -0.010 | 4.021 | 4.792 | 4.067 | 0.595 | 0.619 |
| $k = 60$ | -0.004 | -0.004 | -0.006 | 3.493 | 3.884 | 3.517 | 0.606 | 0.630 |
| Panel 3: $\gamma = 1, (\lambda^{(1)}, \lambda^{(2)}) = (1000, 1000)$ | | | | | | | | |
| $k = 5$ | -0.023 | -0.038 | -0.048 | 9.898 | 16.033 | 10.451 | 0.533 | 0.594 |
| $k = 10$ | -0.014 | -0.020 | -0.026 | 6.194 | 8.789 | 6.367 | 0.563 | 0.604 |
| $k = 30$ | -0.008 | -0.007 | -0.012 | 4.019 | 4.818 | 4.061 | 0.598 | 0.629 |
| $k = 60$ | -0.006 | -0.004 | -0.008 | 3.457 | 3.855 | 3.473 | 0.614 | 0.636 |
| Panel 4: $\gamma = 2, (\lambda^{(1)}, \lambda^{(2)}) = (1000, 1000)$ | | | | | | | | |
| $k = 5$ | -0.031 | -0.040 | -0.055 | 9.738 | 15.468 | 10.241 | 0.549 | 0.613 |
| $k = 10$ | -0.021 | -0.024 | -0.035 | 6.265 | 9.053 | 6.531 | 0.563 | 0.619 |
| $k = 30$ | -0.013 | -0.008 | -0.018 | 3.938 | 4.785 | 4.000 | 0.597 | 0.628 |
| $k = 60$ | -0.012 | -0.006 | -0.014 | 3.393 | 3.846 | 3.433 | 0.612 | 0.641 |

Table S1: Finite-sample bias, variance, and relative mean squared error of $\hat{\rho}_n^*$, $\hat{\rho}_{C,n}$, and $\hat{\rho}_{P,n}$ under the stochastic correlation model with balanced sampling design and measurement error. For each estimator, the relative MSE is calculated relative to that of the benchmark return-based estimator $\hat{\rho}_{C,n}$. All moments are simulated based on 10,000 Monte Carlo realizations. The parameter $\gamma$ controls the noise-to-signal ratio of the measurement error, while $(\lambda^{(1)}, \lambda^{(2)})$ denotes the per-minute average number of Poisson observation arrivals.

| | Bias | | | Variance ×100 | | | Relative MSE | |
|---|---|---|---|---|---|---|---|---|
| | $\hat{\rho}_n^*$ | $\hat{\rho}_{C,n}$ | $\hat{\rho}_{P,n}$ | $\hat{\rho}_n^*$ | $\hat{\rho}_{C,n}$ | $\hat{\rho}_{P,n}$ | $\hat{\rho}_n^*$ | $\hat{\rho}_{P,n}$ |
| Panel 1: $\gamma = 0, (\lambda^{(1)}, \lambda^{(2)}) = (1000, 100)$ | | | | | | | | |
| $k = 5$ | -0.030 | -0.037 | -0.056 | 9.821 | 15.544 | 10.410 | 0.548 | 0.617 |
| $k = 10$ | -0.019 | -0.020 | -0.033 | 6.304 | 8.894 | 6.533 | 0.573 | 0.622 |
| $k = 30$ | -0.014 | -0.009 | -0.020 | 4.102 | 4.866 | 4.172 | 0.619 | 0.660 |
| $k = 60$ | -0.013 | -0.008 | -0.016 | 3.542 | 3.942 | 3.570 | 0.627 | 0.658 |
| Panel 2: $\gamma = 0.5, (\lambda^{(1)}, \lambda^{(2)}) = (1000, 100)$ | | | | | | | | |
| $k = 5$ | -0.035 | -0.038 | -0.060 | 9.952 | 15.580 | 10.533 | 0.562 | 0.637 |
| $k = 10$ | -0.025 | -0.022 | -0.038 | 6.172 | 8.637 | 6.419 | 0.588 | 0.655 |
| $k = 30$ | -0.019 | -0.011 | -0.024 | 3.965 | 4.780 | 4.021 | 0.614 | 0.655 |
| $k = 60$ | -0.017 | -0.008 | -0.020 | 3.439 | 3.863 | 3.463 | 0.638 | 0.670 |
| Panel 3: $\gamma = 1, (\lambda^{(1)}, \lambda^{(2)}) = (1000, 100)$ | | | | | | | | |
| $k = 5$ | -0.039 | -0.040 | -0.066 | 9.472 | 15.473 | 10.066 | 0.551 | 0.624 |
| $k = 10$ | -0.034 | -0.028 | -0.048 | 6.173 | 8.904 | 6.406 | 0.589 | 0.646 |
| $k = 30$ | -0.029 | -0.016 | -0.035 | 3.917 | 4.749 | 3.994 | 0.656 | 0.707 |
| $k = 60$ | -0.028 | -0.015 | -0.031 | 3.332 | 3.827 | 3.373 | 0.693 | 0.735 |
| Panel 4: $\gamma = 2, (\lambda^{(1)}, \lambda^{(2)}) = (1000, 100)$ | | | | | | | | |
| $k = 5$ | -0.077 | -0.057 | -0.101 | 10.073 | 15.828 | 10.483 | 0.618 | 0.690 |
| $k = 10$ | -0.069 | -0.046 | -0.081 | 6.130 | 9.150 | 6.405 | 0.658 | 0.730 |
| $k = 30$ | -0.064 | -0.033 | -0.066 | 3.595 | 4.666 | 3.684 | 0.813 | 0.853 |
| $k = 60$ | -0.063 | -0.030 | -0.063 | 3.011 | 3.714 | 3.081 | 0.985 | 1.002 |

Table S2: Finite-sample bias, variance, and relative mean squared error of $\hat{\rho}_n^*$, $\hat{\rho}_{C,n}$, and $\hat{\rho}_{P,n}$ under the stochastic correlation model with extreme observation asynchronicity and measurement error. For each estimator, the relative MSE is calculated relative to that of the benchmark return-based estimator $\hat{\rho}_{C,n}$. All moments are simulated based on 10,000 Monte Carlo realizations. The parameter $\gamma$ controls the noise-to-signal ratio of the measurement error, while $(\lambda^{(1)}, \lambda^{(2)})$ denotes the per-minute average number of Poisson observation arrivals.

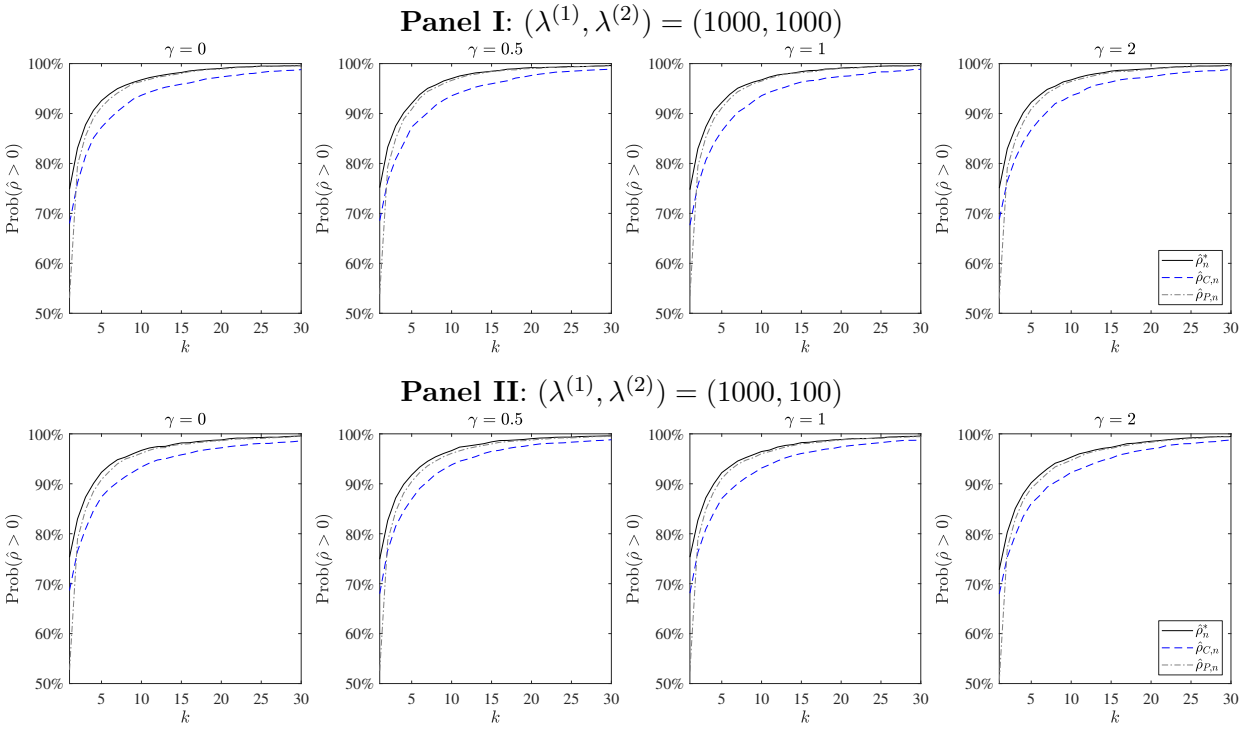


Figure S2: Finite-sample sign accuracies of $\hat{\rho}_n^*$, $\hat{\rho}_{C,n}$, and $\hat{\rho}_{P,n}$ under the stochastic correlation model with the balanced setting $(\lambda^{(1)}, \lambda^{(2)}) = (1000, 1000)$ and the extreme asynchronicity setting $(\lambda^{(1)}, \lambda^{(2)}) = (1000, 100)$. The parameter $\gamma$ controls the noise-to-signal ratio of the measurement error. The vertical axis reports the simulated probability that each estimator correctly identifies the sign of $\rho_0 > 0$.

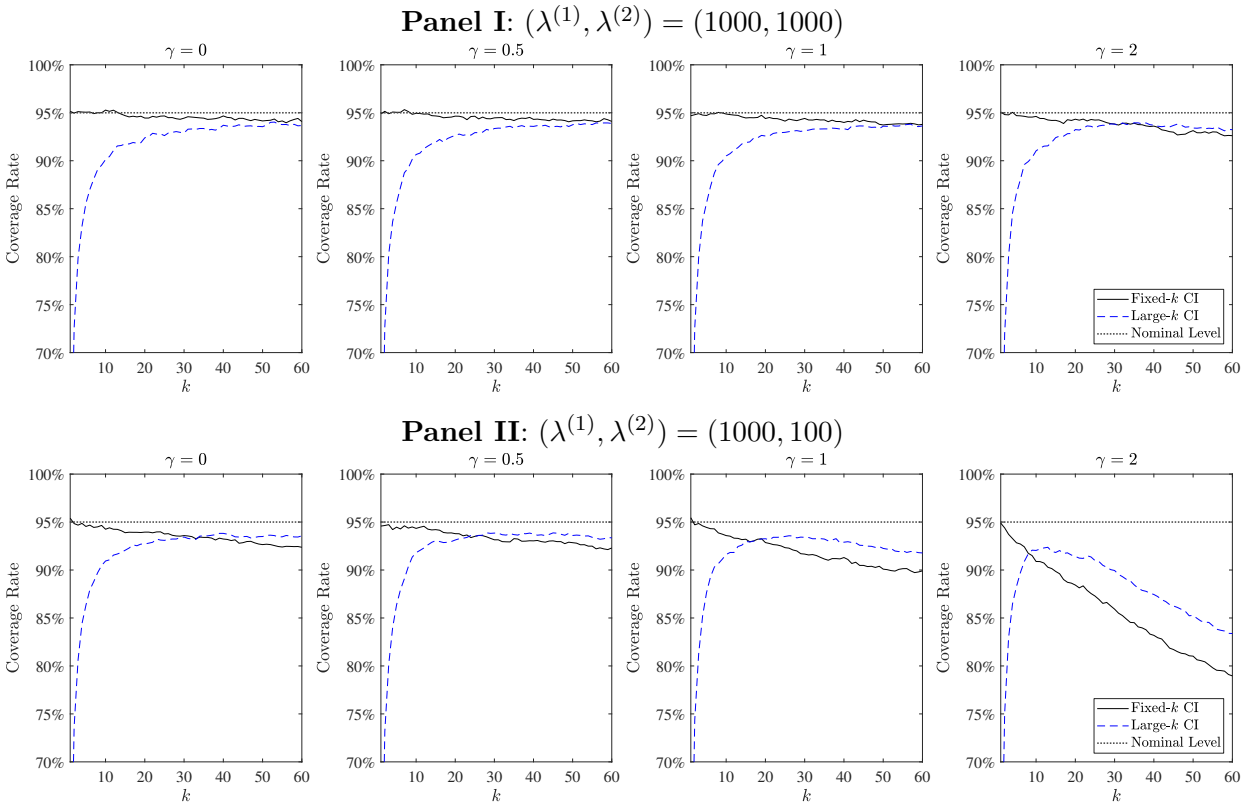


Figure S3: Finite-sample coverage rates of 95%-level large-$k$ and fixed-$k$ confidence intervals under the stochastic correlation model with the balanced setting $(\lambda^{(1)}, \lambda^{(2)}) = (1000, 1000)$ and the extreme asynchronicity setting $(\lambda^{(1)}, \lambda^{(2)}) = (1000, 100)$. The parameter $\gamma$ controls the noise-to-signal ratio of the measurement error.